Supporting Information

$Fe_2(MoO_4)_3$ assembled by cross-stacking of porous nanosheets enables a high-performance aluminum-ion battery

Huanyu Liang, ‡[a] Yongshuai Liu, ‡[a] Fengkai Zuo,[a] Cunliang Zhang,*[b] Li Yang,[a] Linyi Zhao,[a] Yuhao Li,[a] Yifei Xu,[a] Tiansheng Wang,[a] Xia Hua,[a] Yue Zhu*[c] and Hongsen Li*[a]

[a] College of Physics, Center for Marine Observation and Communications, Qingdao University. Qingdao 266071, P. R. China

[b] School of Chemistry and Chemical Engineering, Henan Engineering Center of New Energy Battery Materials, Henan Key Laboratory of Bimolecular Recognition and Sensing, Shangqiu Normal University, Shangqiu, Henan 476000, P. R. China

[c] Max Planck Institute for Solid State Research, Heisenbergstraße 1, 70569 Stuttgart, Germany

* Corresponding authors: hsli@qdu.edu.cn; y.zhu@fkf.mpg.de; zcliang@126.com;
‡ These authors contribute equally to this work.

Experimental Section

***Preparation of P-FMO*:** P-FMO was fabricated by a facile solvothermal method. In a typical synthesis, 0.8 g $Fe(NO_3)_3 \cdot 9H_2O$ and 1 g $Na_2MoO_4 \cdot 2H_2O$ were dissolved in 20 mL ethylene glycol, respectively. The resulting solution was mixed under continuous stirring for 30 min at room temperature. Later, the above mixture was transferred into a 60 mL Teflon-lined autoclave and kept 200 ^oC for 15 h. A gray precipitate, name P-FMO precursor, was collected by centrifugation, and washed with deionized water three times and rinsed with ethanol one time. The P-FMO precursor was dried at 60 ^oC in a vacuum oven for 12 h. Finally, the P-FMO sample was harvested by calcination P-FMO precursor at 500 ^oC for 10 h in air atmosphere with a heating rate of 2 $^oC\ min^{-1}$.

Materials characterization: The crystal phases of as-prepared P-FMO were detected by powder X-ray diffraction (Rigaku Ultima IV, Cu Kα). The FESEM images of P-FMO were characterized by a ZEISS Sigma-300. Transmission electron microscope (TEM), Field-emission scanning electron microscopy (FESEM) and energy dispersive X-ray spectroscopy (EDS) were employed to describe the morphologies and structures of the samples. X-ray photoelectron spectroscopy (XPS, ESCALAB 250Xi) was performed to characterize the valence states of Fe and Mo in different reaction states. The N_2 adsorption/desorption isotherms of as-prepared materials were conducted on ASAP 2010.

Electrochemical measurements: Swagelok-type cell assembly protocols were

performed in an Ar-purged glove box with H_2O and O_2 contents less than 0.1 ppm. For electrode fabrication, pristine P-FMO was blended with Super P carbon black and Carboxymethyl cellulose (CMC) to obtain a final mass ratio of active material: carbon: binder in the cathode of 70: 20: 10. The mixture was suspended in distilled water to obtain a glutinous slurry, which was then coated on tantalum foils. Note that tantalum foil was preferred to molybdenum foil as current collector to avoid the influence of collector on P-FMO. Electrodes with diameter of 10 mm were punched and dried at 60 ^oC under vacuum for 12 h. Al foil (99.99%) and Whatman GF/C type glass fiber paper were employed for the counter electrode and separator, respectively. The electrolyte was ionic liquid (IL) in mixture of $AlCl_3$ and [EMIm]Cl with a 1.3 ratio. Charge and discharge were implemented between 0.01 V as the lower limit and 2.2 V as the upper limit. The cyclic voltammetry (CV) scan was conducted using an electrochemical workstation (IVIUM technologies).

Ex-situ technical observation: XPS, XRD and TEM measurements were characterized on charged/discharged P-FMO electrodes to ascertain the phase state upon alkali-ion extraction and reinsertion in aluminum-ion battery. Electrochemical measurements were stopped upon discharging the electrode at 0.01 V and charging others electrodes at 2.2 V in the first cycle. The cells were dismantled, and the electrodes were washed for several times using PC and dried in vacuum for 12 h.

Computational methods: All the calculations were performed within the framework of the density functional theory (DFT) as implemented in the Vienna Ab initio Software Package (VASP 5.4.4) code within the Perdew-Burke-Ernzerhof (PBE)

generalized gradient approximation and the projected augmented wave (PAW) method.[1] The cutoff energy for the plane-wave basis set was set to 450 eV. The ultrasoft pseudo-potential was employed to describe the interaction between valence electrons and the ionic core. Monkhorst-Pack special k-point meshes of 3 × 3 × 1 were proposed to carry out geometry optimization and electronic structure calculation. During the geometry optimization, all atoms were allowed to relax without any constraints until the convergence thresholds of maximum force and energy were smaller than 0.01 eV/Å and 1.0×10^{-5} eV/atom, respectively. A vacuum layer of 12 Å was introduced to avoid interactions between periodic images. The climbing image nudged elastic band (CI-NEB)[2] method was used to confirm the transition states with only one imaginary frequency along the reaction coordinates.

Supplementary Figures and Tables

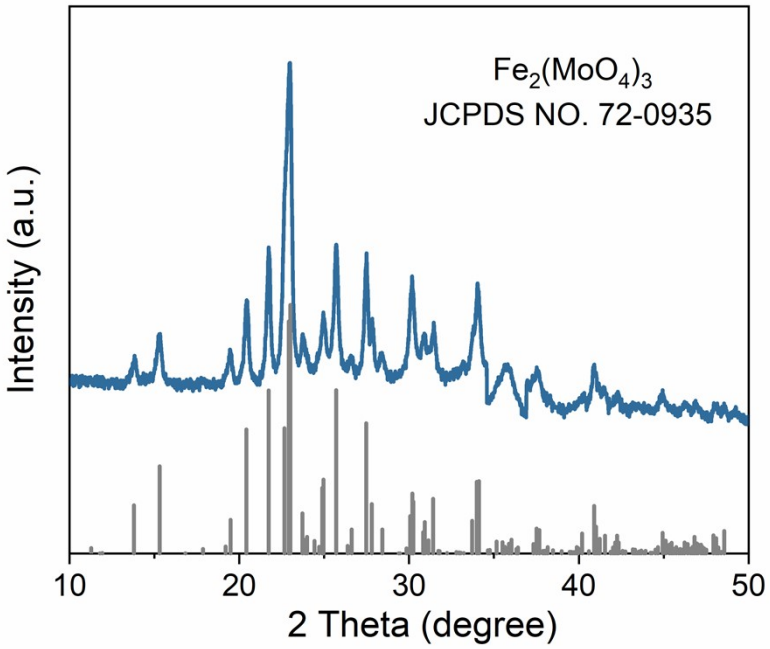

Fig. S1. XRD pattern of the P-FMO material.

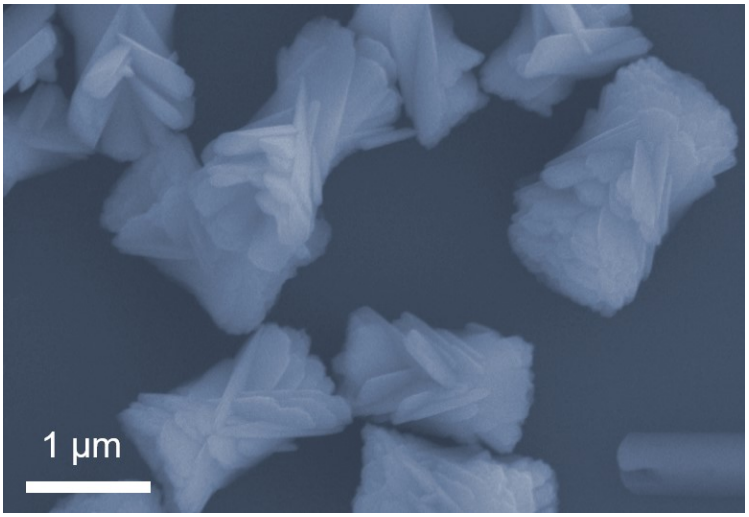

Fig. S2. FESEM images of P-FMO precursor.

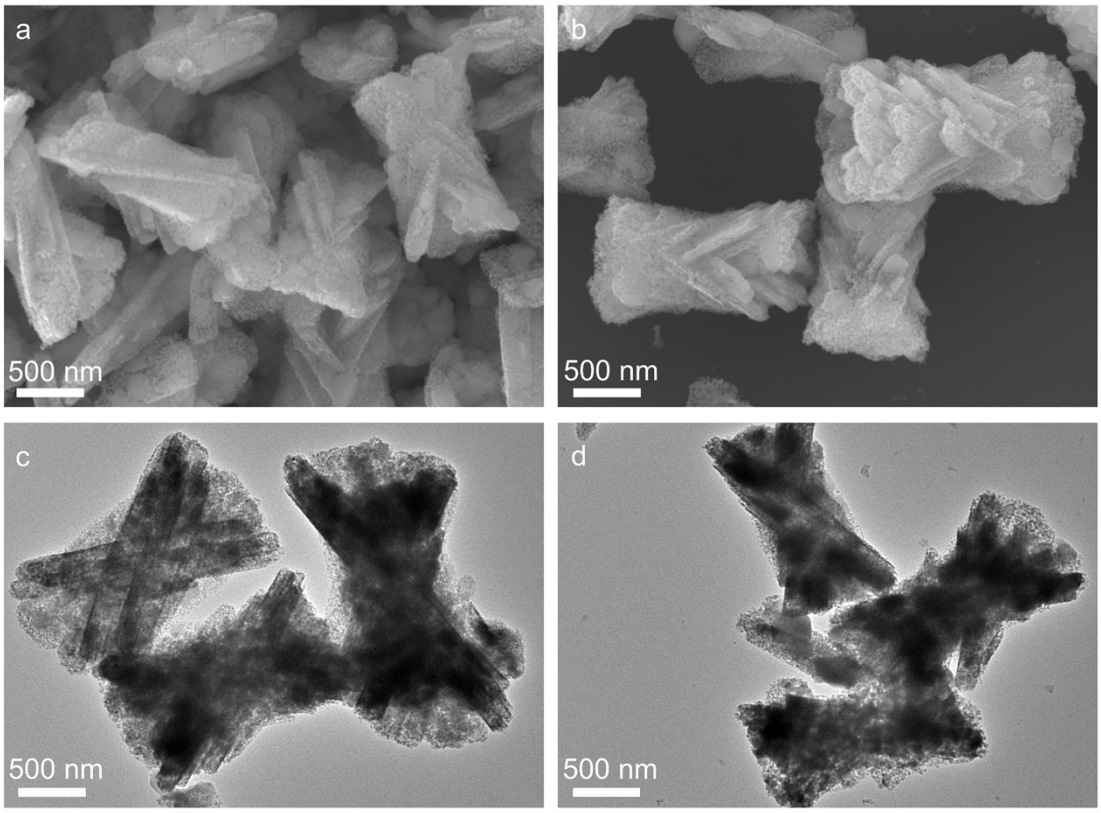

Fig. S3. a, b) FESEM images of P-FMO. c, d) TEM images of P-FMO.

Note to Fig. S3. The large-scale images in Fig. S3 reveal the good uniformity of the as-synthesized P-FMO.

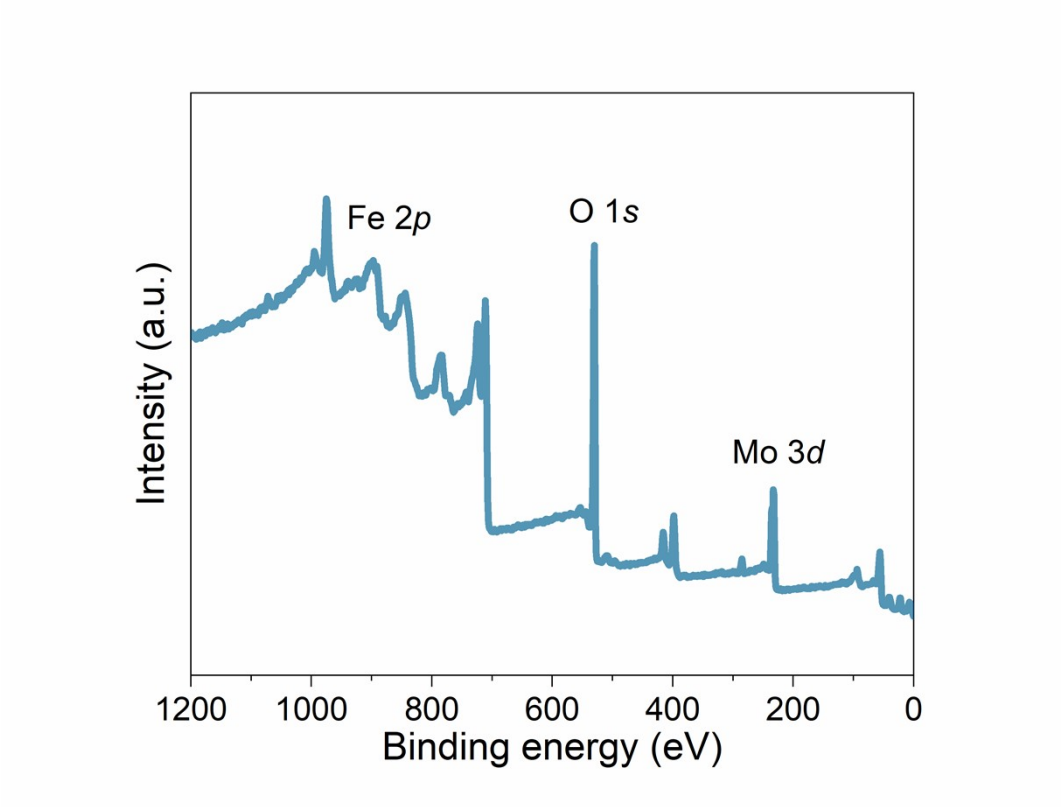

Fig. S4. The XPS spectra of P-FMO.

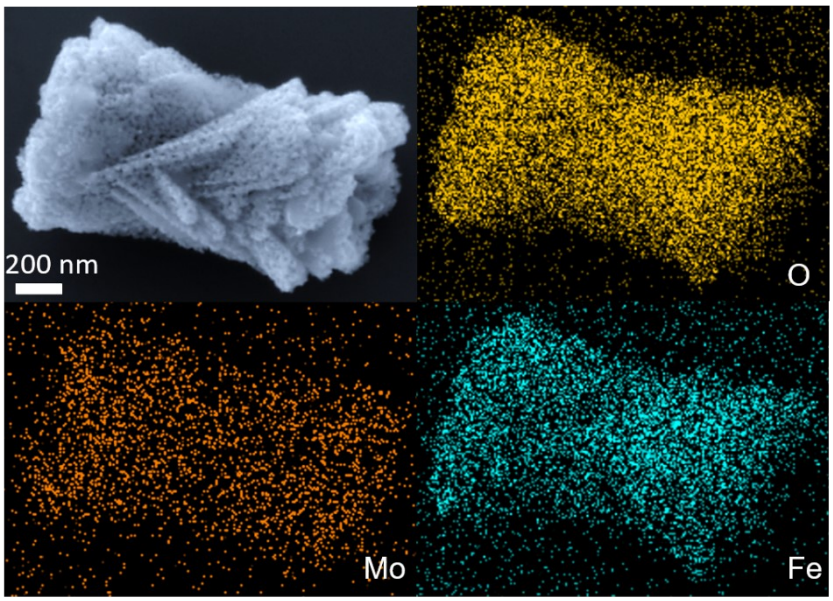

Fig. S5. EDS mapping images of P-FMO.

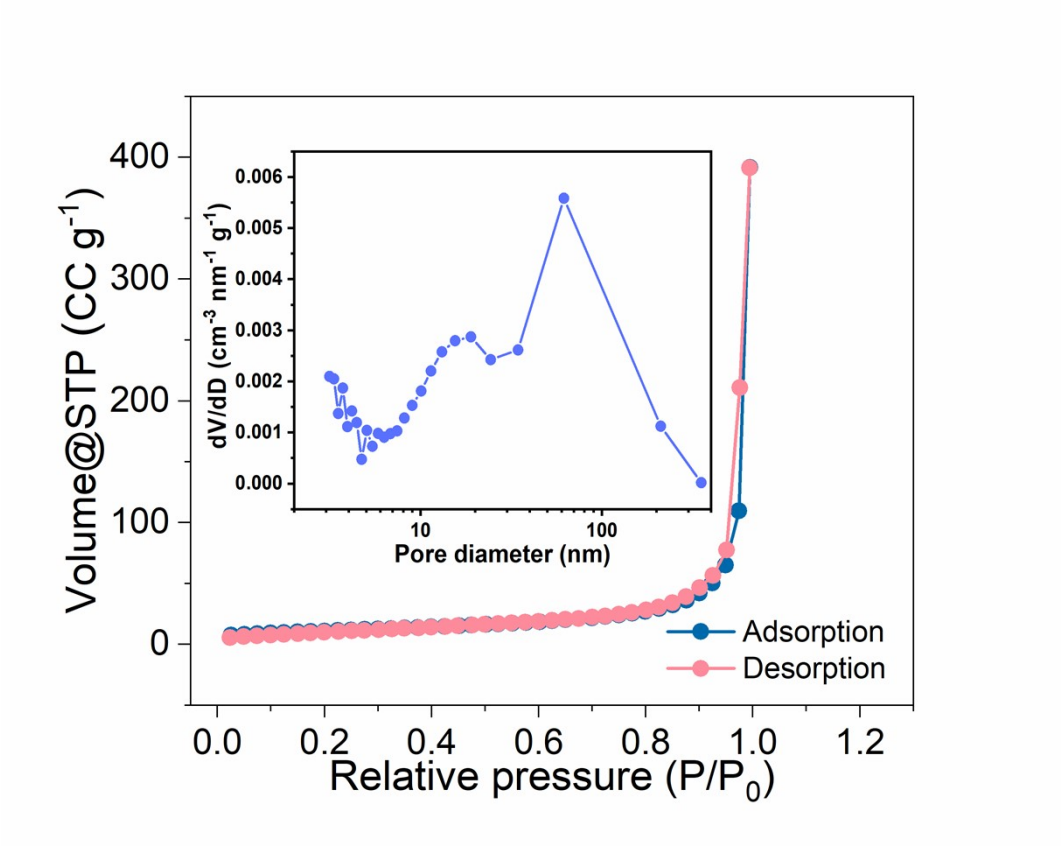

Fig. S6. N_2 adsorption-desorption isotherms and pore size distribution of P-FMO.

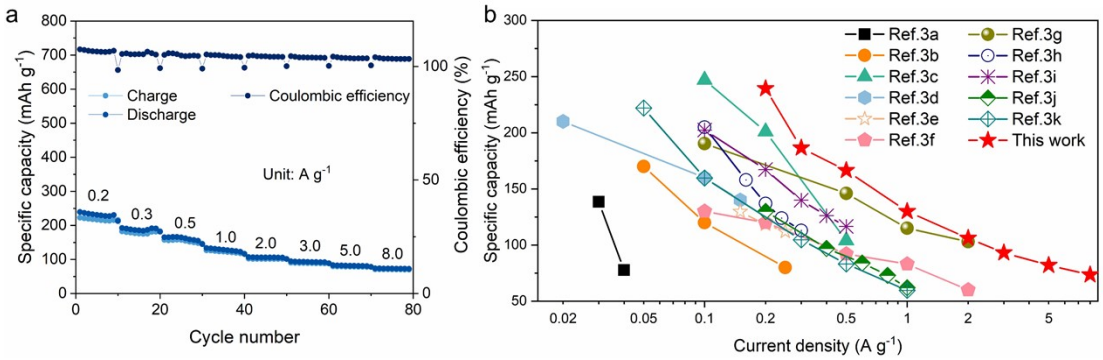

Fig. S7. a) Rate performance with rates ranging from 0.2 to 8.0 A g^{-1}. b) Comparison of the Ragone plot of the $Fe_2(MoO_4)_3$ AIBs with other reported positive electrode materials.

Note to Fig. S7. The well-designed P-FMO electrode exhibits superior rate capability (Fig. S7a). Fig. S7b shows the comparison of the rate capability with the state-of-the-art results in previous studies on AIBs[3], demonstrating the superior rate capability in this work with regard to recently reported works.

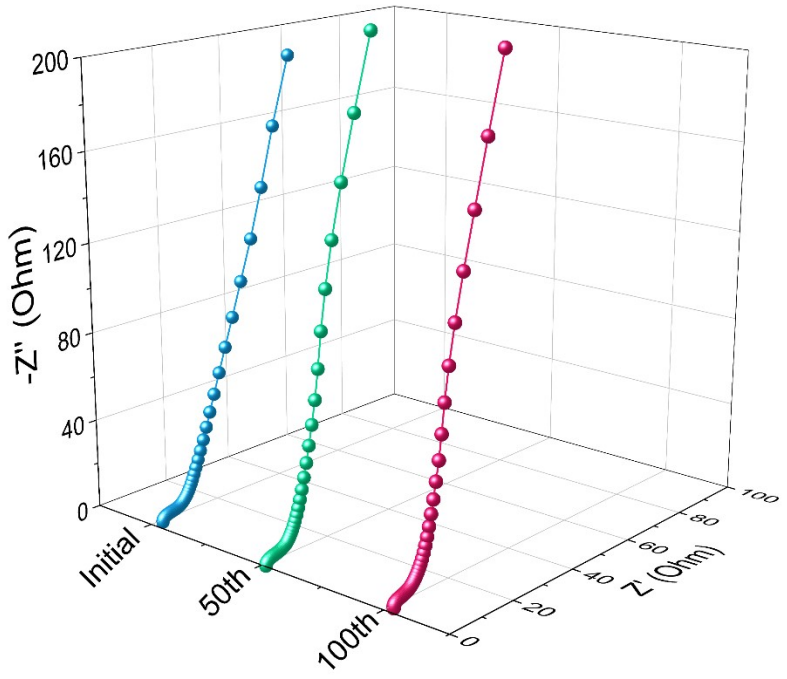

Fig. S8. Electrochemical impedance spectra at different cycles of P-FMO.

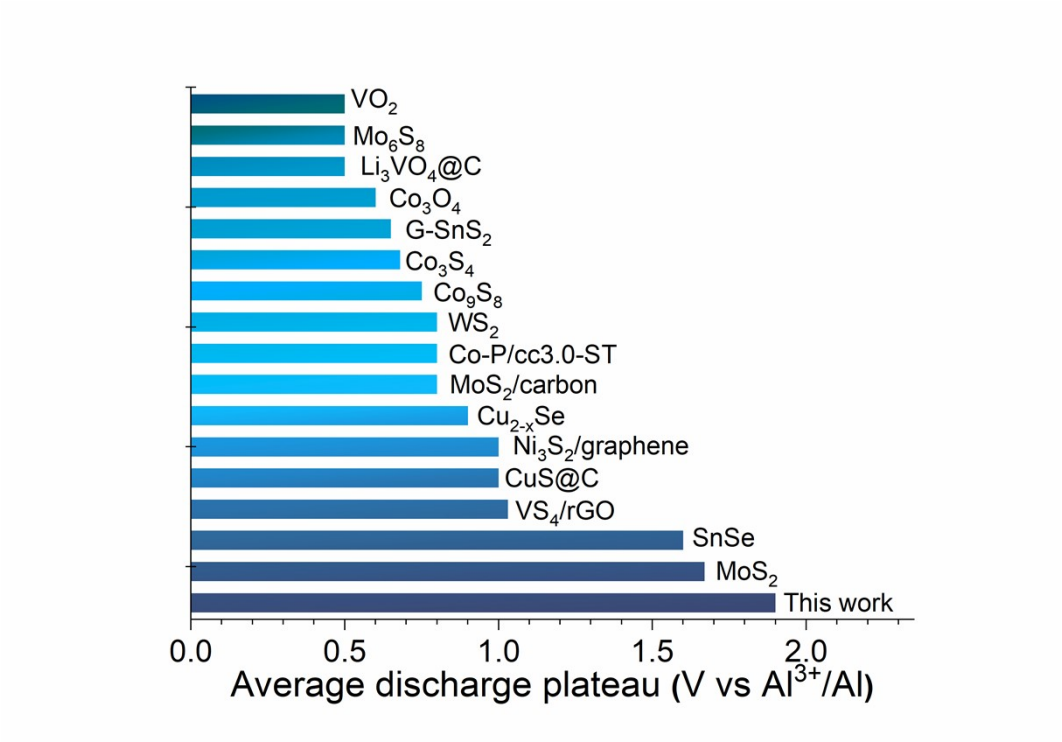

Fig. S9. Comparison of discharge plateau of different cathode materials for Al-ion batteries.

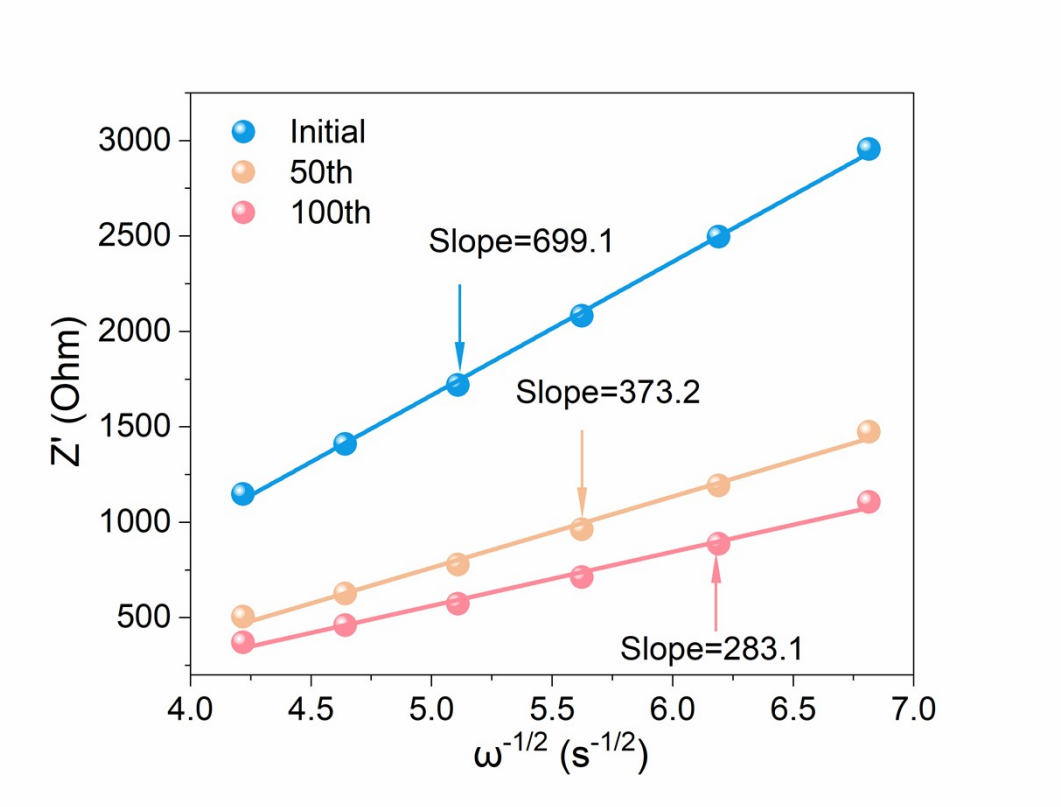

Fig. S10. The relationship between Z′ and $w^{-1/2}$ in low-frequency range.

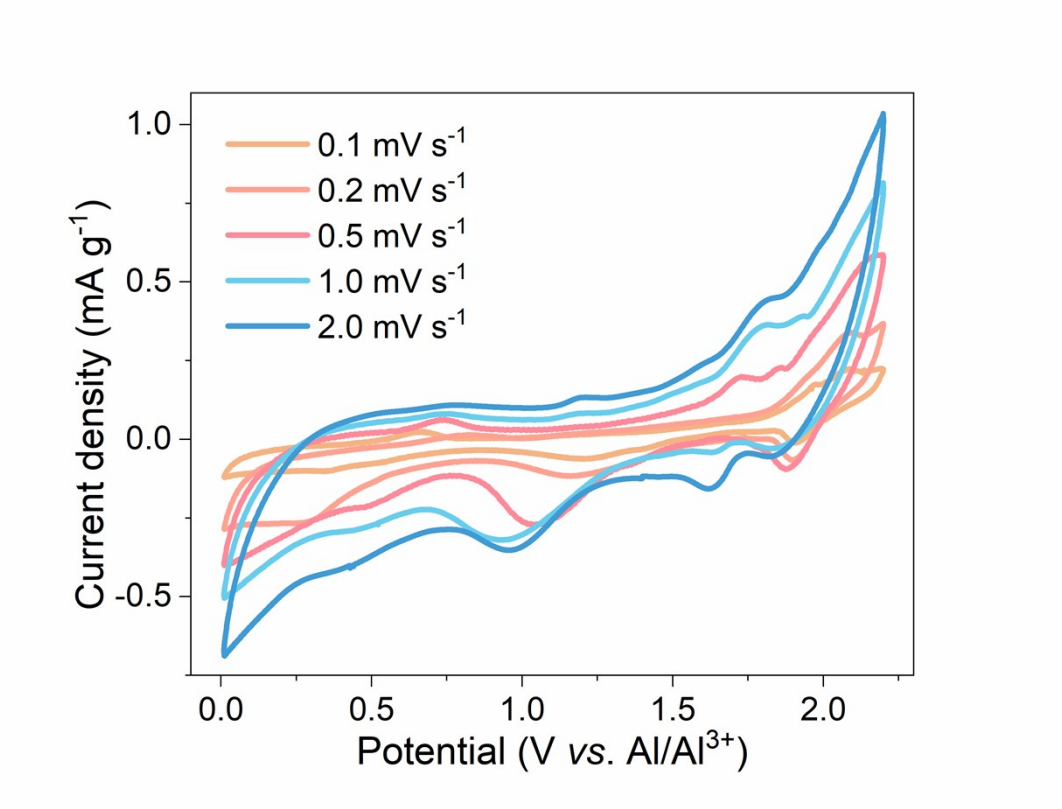

Fig. S11. Cyclic voltammetry curves from 0.1 to 2.0 mV s^{-1} of the P-FMO electrode.

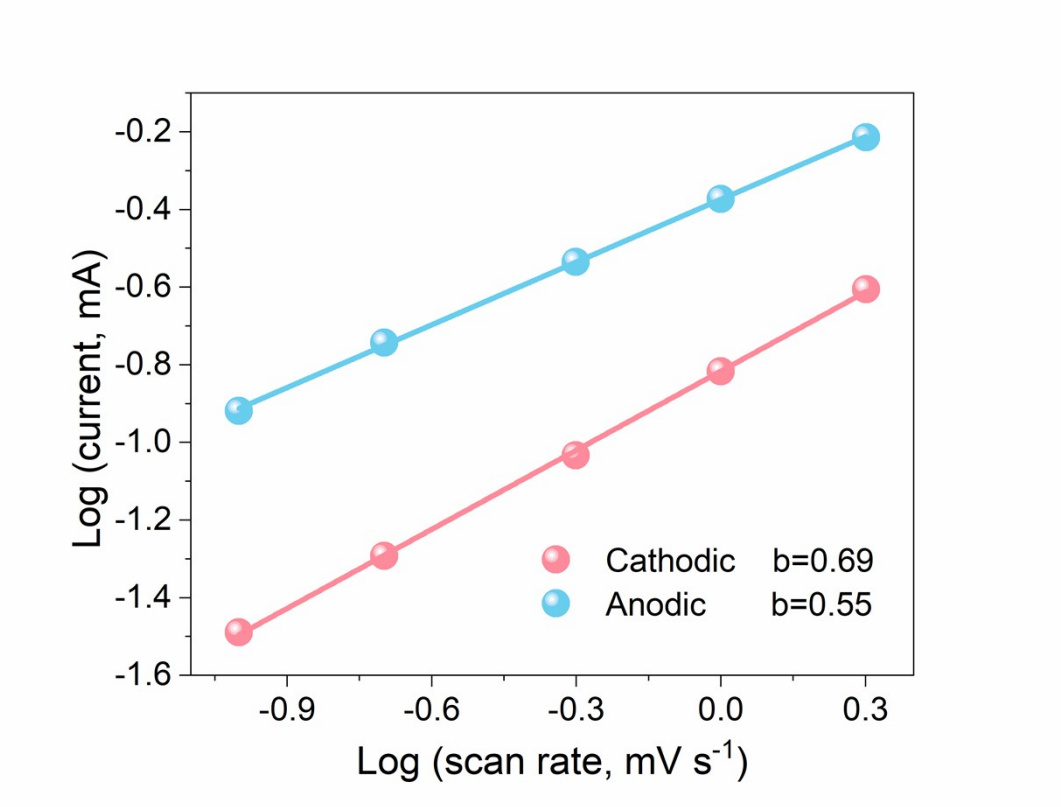

Fig. S12. The linear relationship of peak currents and scan rates of P-FMO electrode.

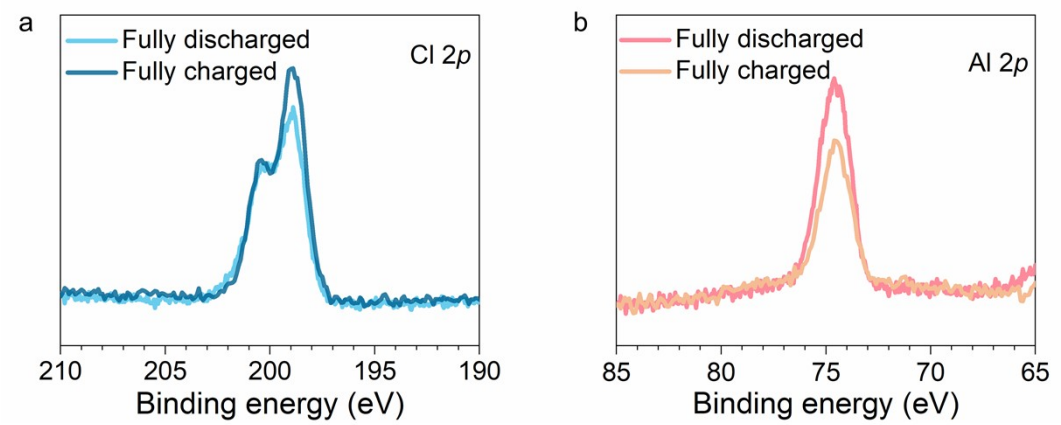

Fig. S13. *Ex-situ* XPS spectra of the (a) Al 2*p*, and (b) Cl 2*p* peaks for fully discharged and charged P-FMO electrodes, respectively.

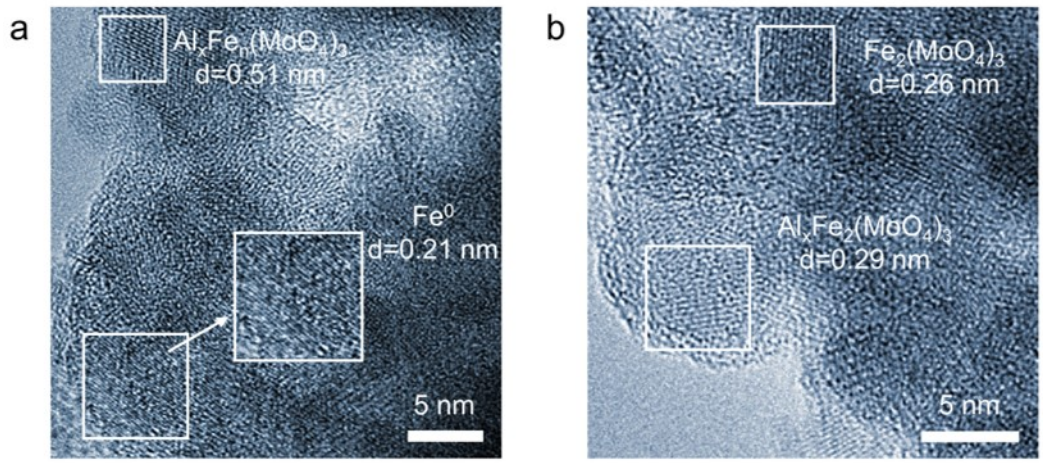

Fig. S14. HRTEM of P-FMO electrodes at (a) 0.01 V and (b) 2.2 V.

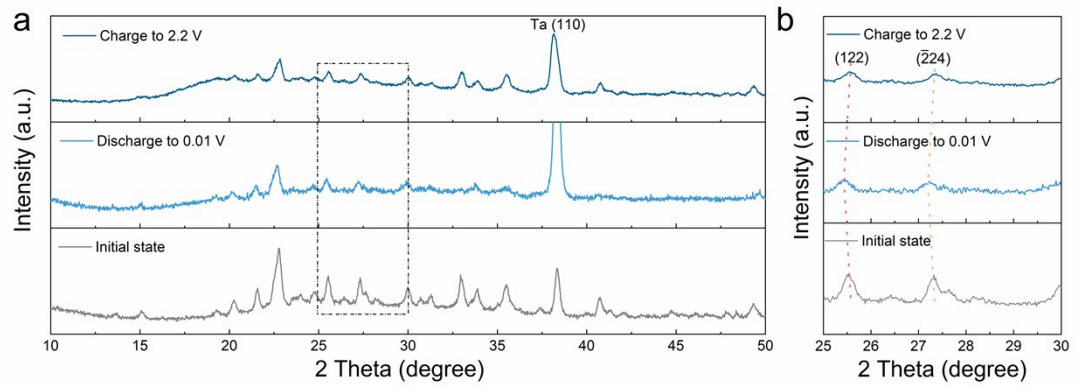

Fig. S15. *Ex-situ* XRD pattern under different states.

Table S1. Comparison of some typical chalcogenide-based cathode materials in terms of specific capacity and cycling stability for AIBs.

Type of materials	***Cycle number***	***Current density: mA g^{-1}***	***Specific capacity: mAh g^{-1}***	***Ref.***
MoS_2	100	40	66.7	[3a]
WS_2	500	1000	119	[4]
Co_3O_4	100	200	122.1	[5]
VO_2	100	50	116	[6]
VS_4/rGO	100	300	60	[7]
Ni_3S_2/graphene	100	100	60	[8]
Co_3S_4	150	50	90	[3b]
$Cu_{2-x}Se$	100	200	100	[3c]
Mo_6S_8	50	12	70	[9]
G-SnS_2	100	200	70	[10]
SnSe	100	300	107	[11]
CuS@C	100	20	90	[3d]
Co-P/cc3.0-ST	400	200	85.1	[12]
MoS_2/carbon	200	100	126.6	[3e]
Co_9S_8	250	200	120	[3f]
Li_3VO_4@C	100	20	48	[13]
P-FMO	**2000**	**1000**	**126.5**	**This work**

Table S2. Calculated formation energy for $Fe_2(MoO_4)_3$, $Fe_2(MoO_4)_3$ Al and $Fe_2(MoO_4)_3$ ($AlCl_4$).

Compound	Formation energy (eV)
$Fe_2(MoO_4)_3$	-----
$Fe_2(MoO_4)_3$ Al	-2.859
$Fe_2(MoO_4)_3$ ($AlCl_4$)	1.08

References

[1] a) J. P. Perdew, K. Burke, M. Ernzerhof, *Phys. Rev. Lett.* **1996**, *77*, 3865-3868; b) B. Hammer, L. B. Hansen, J. K. Nørskov, *Phys. Rev. B* **1999**, *59*, 7413-7421; c) P. E. Blöchl, *Phys. Rev. B* **1994**, *50*, 17953-17979; d) G. Kresse, D. Joubert, *Phys. Rev. B* **1999**, *59*, 1758-1775.

[2] a) G. Henkelman, H. Jónsson, *J. Chem. Phys.* **2000**, *113*, 9978-9985; b) G. Henkelman, B. P. Uberuaga, H. Jónsson, *J. Chem. Phys.* **2000**, *113*, 9901-9904; c) D. Sheppard, G. Henkelman, *J. Comput. Chem.* **2011**, *32*, 1769-1771.

[3] a) Z. Li, B. Niu, J. Liu, J. Li, F. Kang, *ACS Appl. Mater. Interfaces* **2018**, *10*, 9451-9459; b) H. Li, H. Yang, Z. Sun, Y. Shi, H.-M. Cheng, F. Li, *Nano Energy* **2019**, *56*, 100-108; c) J. Jiang, H. Li, T. Fu, B.-J. Hwang, X. Li, J. Zhao, *ACS Appl. Mater. Interfaces* **2018**, *10*, 17942; d) S. Wang, S. Jiao, J. Wang, H.-S. Chen, D. Tian, H. Lei, D.-N. Fang, *ACS Nano* **2017**, *11*, 469-477; e) W. Yang, H. Lu, Y. Cao, B. Xu, Y. Deng, W. Cai, *ACS Sustain. Chem. Eng*. **2019**, *7*, 4861-4867; f) Z. Hu, K. Zhi, Q. Li, Z. Zhao, H. Liang, X. Liu, J. Huang, C. Zhang, H. Li, X. Guo, *J. Power Sources* **2019**, *440*, 227147; g) Q. Zhou, D. Wang, Y. Wang, L. Ni, H. Zhang and J. Zhao, *J. Phys. Chem. C*, **2022**, *126*, 2679-2688; h) J. Zhang, L. Zhang, Y. Zhao, J. Meng, B. Wen, K. M. Muttaqi, M. R. Islam, Q. Cai and S. Zhang, *Adv. Energy Mater*., **2022**, *12*, 2200959; i) Y. Wang, J. Cai, T. Han, C. Hu, Y. Zhu, J. Li and J. Liu, *Appl. Surf. Sci*., **2022**, *591*, 153157; j) Y. Liu, Y. Li, F. Zuo, J. Liu, Y. Xu, L. Yang, H. Zhang, H. Wang, X. Zhang, C. Liu, Q. Li and H. Li, *Small*, **2022**, *18*, e2203236; k) S. Ju, J. Ye, Y. Meng, G. Xia and X. Yu, *Adv. Energy Mater*., **2022**, *12*, 2201653.

[4] Z. Zhao, Z. Hu, Q. Li, H. Li, X. Zhang, Y. Zhuang, F. Wang, G. Yu, *Nano Today* **2020**, *32*, 100870.

[5] J. Liu, Z. Li, X. Huo, J. Li, *J. Power Sources* **2019**, *422*, 49-56.

[6] W. Wang, B. Jiang, W. Xiong, H. Sun, Z. Lin, L. Hu, J. Tu, J. Hou, H. Zhu, S. Jiao, *Sci. Rep*. **2013**, *3*, 3383.

[7] X. Zhang, S. Wang, J. Tu, G. Zhang, S. Li, D. Tian, S. Jiao, *ChemSusChem* **2018**, *11*, 709-715.

[8] S. Wang, Z. Yu, J. Tu, J. Wang, D. Tian, Y. Liu, S. Jiao, *Adv. Energy Mater*. **2016**, *6*, 1600137.

[9] L. Geng, G. Lv, X. Xing, J. Guo, *Chem. Mater*. **2015**, *27*, 4926-4929.

[10] Y. Hu, B. Luo, D. Ye, X. Zhu, M. Lyu, L. Wang, *Adv. Mater*. **2017**, *29*, 1606132.

[11] Y. Zhang, B. Zhang, J. Li, J. Liu, X. Huo, F. Kang, *Chem. Eng. J*. **2021**, *403*, 126377.

[12] S. Lu, M. Wang, F. Guo, J. Tu, A. Lv, Y. Chen, S. Jiao, *Chem. Eng. J*. **2020**, *389*, 124370.

[13] J. Jiang, H. Li, J. Huang, K. Li, J. Zeng, Y. Yang, J. Li, Y. Wang, J. Wang, J. Zhao, *ACS Appl. Mater. Interfaces* **2017**, *9*, 28486-28494.